PERGAMON

International Journal of Heat and Mass Transfer 43 (2000) 1749–1758

International Journal of HEAT and MASS TRANSFER

www.elsevier.com/locate/ijhmt

Limiting behavior of turbulent scalar transport close to a wall

Y. Na, T.J. Hanratty*

Department of Chemical Engineering, University of Illinois at Urbana-Champaign, 205 Roger Adams Laboratory, Box C-3, 600 South Mathews Avenue, Urbana, IL 61801-3792, USA

Received 4 January 1999; received in revised form 11 August 1999

Abstract

A direct numerical simulation of fully developed turbulent flow in a channel is used to study passive scalar transport in the immediate vicinity of a wall. The Reynolds number, based on the channel half-height and friction velocity, is 150 and the Prandtl number is varied from 1 to 10. DNS results and experimental measurements of mass transfer rates at high Schmidt numbers are used to investigate the effect of Schmidt or Prandtl number. The wavenumber spectra for temperature fluctuations show a damping of the contributions of large wavenumbers with increasing Schmidt or Prandtl number. This result suggests that the analogy between momentum and scalar transport cannot be used to define the limiting behavior of turbulent diffusivity for $y \to 0$. Furthermore, this limiting relation cannot be used to calculate the concentration or temperature profile since it is applicable only in the conductive sublayer, where turbulent transport is not important.

Keywords: Turbulent transfer; Large Prandtl number; Large Schmidt number; Direct numerical solutions; Channel flow; Limiting behavior close to wall

1. Introduction

One of the ingredients in understanding turbulent transport of a scalar between a flowing fluid and a flat solid surface is the definition of the limiting behavior of the fluctuating temperature and velocity fields close to a wall. This understanding becomes particularly important at high Schmidt (Sc) or Prandtl (Pr) numbers, for which almost all of the change of mean temperature or concentration can occur in the viscous sublayer. The usual approach is to employ Taylor series representations of the velocity and scalar fields in the neighborhood of $y \to 0$, where y is the distance from the wall [1–3]. This has led to the finding that the turbulent kinematic viscosity, ν^t, varies as y^3 for $y \to 0$. The use of the analogy between momentum and scalar transport then gives the turbulent diffusivity as $D^t \sim y^3$, with the proportionality constant being independent of Pr or Sc. This result has been widely used in heat transfer studies [4]. At large Pr it has been assumed to define turbulent transport throughout the entire temperature profile.

Mass transfer data at large Sc have been interpreted by assuming $D^t \sim y^m$ over the whole concentration boundary layer where $m = 3$ or 4 [1,5–8] and the proportionality constant is independent of Sc. A mass balance equation gives $K/u^* \sim Sc^{-(m-1/m)}$, where K is the mass transfer coefficient and u^* is the friction velocity. Electrochemical methods have been used to obtain

* Corresponding author. Tel.: +1-217-333-1318; fax: +1-217-333-5052.

E-mail address: hanratty@scs.uiuc.edu (T.J. Hanratty).

0017-9310/00/$ - see front matter
PII: S0017-9310(99)00258-6

Nomenclature

c	fluctuation in the concentration
$\bar{C}$	time-averaged local concentration
c_p	specific heat at constant pressure
D	molecular diffusivity
D^t	turbulent diffusivity
H	half channel height normalized with wall variables
k	fluctuation in the mass transfer coefficient normalized by the friction velocity
K	mass transfer coefficient
$\bar{K}$	time-averaged mass transfer coefficient
k_x	streamwise wavenumber normalized with wall variables
n	frequency normalized with wall variables
P	pressure
P_x	streamwise pressure gradient
Pr	Prandtl number
Pr^t	turbulent Prandtl number
q	local heat flux
q_w	heat flux at the channel wall
Sc	Schmidt number
$R_{\theta v}$	correlation coefficient between θ and v
T	temperature normalized by the friction temperature $= \bar{T} + \theta$
$\bar{T}$	mean temperature normalized by the friction temperature
T_w	temperature at the wall
T^*	friction temperature $= q_w/\rho c_p u^*$
t	time
$\mathbf{u}$	velocity vector in wall units
u, v, w	fluctuating velocity components in wall units in the x, y, z directions
u^*	friction velocity
$\bar{U}$	mean streamwise velocity normalized by the friction velocity
U_c	convection velocity of temperature field normalized by the friction velocity
U_o	centerline velocity normalized by the friction velocity
W_{kk}	spectral density function for $\overline{k^2}$ normalized with wall variables
W_{uv}	spectral density function for v normalized with wall parameters
$W_{\theta\theta}$	spectral density function for $\overline{\theta^2}$ normalized with wall variables
$W_{\theta v}$	co-spectral density function for $\overline{\theta v}$ normalized with wall variables
x, y, z	streamwise, normal and spanwise coordinates in wall units

Greek symbols

Δ_θ	thickness of the conductive layer
ν	kinematic viscosity
ν^t	turbulent kinematic viscosity
$\boldsymbol{\omega}$	vorticity vector
Π	pseudo pressure
$\phi(k_x, n)$	two-dimensional spectral density function for $\bar{\theta}^2$
ρ	fluid density
θ	fluctuating temperature normalized by the friction temperature

measurements of mass transfer rates [9–11] at large Schmidt numbers. They give the surprising (and, maybe, controversial) results that $K/u^* \sim Sc^{-0.7}$ and that m is not a whole number. This finding is hard to reconcile with the Taylor series approach outlined in the paragraph above. Consequently, there has been a need to examine more carefully the limiting behavior of the scalar and velocity fields in the limit of $y \to 0$.

This paper uses direct numerical simulations at $Pr = 1$, 3 and 10 to look at the effect of Prandtl number on the spatial variation of the mean-square of the fluctuating temperature, $\overline{\theta^2}$, of the Reynolds transport, $\overline{\theta v}$, and of the turbulent diffusivity in the immediate vicinity of the wall. The system considered is the fully developed velocity and temperature fields that exist in a channel in which the bottom wall is held at temperature $+T_w$ and the top wall at $-T_w$. The Reynolds number, based on the half height of the channel, and the centerline velocity is 2670. Since the velocity and temperature fields are fully developed, heat fluxes at different distances from the wall are the same.

The dimensionless mean square temperature fluctuations, $\overline{\theta^2}/\bar{T}^2$, the correlation coefficient, $R_{\theta v}$, and turbulent diffusivity are found to decrease with increasing Prandtl number for $y \to 0$. These results are explained by examining the wavenumber spectra for $\overline{\theta v}$ and θ^2. Close to the wall, these show a damping of the contributions of large wavenumbers, as had previously been suggested by Shaw and Hanratty [9], by Campbell and Hanratty [10] and by Hanratty and Vassiliadou [11]. These results lead to the conclusion that the analogy between momentum and scalar transport cannot be used to define the limiting behavior of the turbulent diffusivity for $y \to 0$.

The relationship of this work to previous treatments of scalar transfer at large Schmidt or Prandtl numbers is also explored. The practice of representing the turbulent diffusivity as being proportional to the turbulent viscosity, obtained from its limiting relation, can be criticized on two counts: (1) The turbulent Schmidt or Prandtl number is affected by the molecular Schmidt or Prandtl number. (2) The limiting relation for scalar transport holds only in a region where turbulent transport is negligible compared to molecular transport, and not over the entire scalar boundary layer. A consequence is that the usual practice of assuming that the dimensionless transport rate varies as $Sc^{-2/3}$ or $Sc^{-3/4}$ at large Sc or Pr does not have a theoretical foundation. Some speculative arguments are presented to justify the empirical relation, $D^{t} \sim y^{3.38}$, given by Shaw and Hanratty [9] and by Papavassiliou and Hanratty [12,13] to represent turbulent concentration profiles at very large Sc or Pr.

2. Methodology

Numerical solutions are obtained for the three-dimensional, time-dependent Navier–Stokes equation in a skew-symmetric form and for the advection-diffusion equation.

$$\frac{\partial \mathbf{u}}{\partial t} = (\mathbf{u} \times \boldsymbol{\omega}) - \nabla \Pi - P_x e_x + \nabla^2 \mathbf{u} \tag{1}$$

$$\frac{\partial T}{\partial t} - \mathbf{u} \cdot \nabla T + \frac{1}{Pr} \nabla^2 T, \tag{2}$$

where

$$\omega = \nabla \times \mathbf{u} \tag{3}$$

$$\Pi = P - P_x x + \frac{\mathbf{u} \cdot \mathbf{u}}{2} \tag{4}$$

and $\mathbf{u}$ and P denote the velocity vector and the static pressure. All variables are made dimensionless by using wall variables. Solutions of Eqs. (1) and (2) are obtained, which are periodic in the streamwise and spanwise directions, by using the algorithm described by Lyons et al. [14]. The Reynolds number based on the friction velocity, u^*, and the half-channel height, H, is 150. In presenting the results, x, y, z and u, v, w represent coordinates and velocity components made dimensionless by wall variables in the streamwise, the wall-normal and the spanwise directions. Temperature T is made dimensionless with the friction temperature, $T^* = q_w/\rho c_p u^*$.

The results for $Pr = 10$ are for an x, y, z grid of $128 \times 193 \times 128$. The resolution in the y-direction varied from $\Delta y = 0.02$ at the wall to $\Delta y = 2.45$ at the center of the channel. The resolutions in the x and z directions were $\Delta x = 15$, $\Delta z = 7.5$, respectively. A time of about 800 ν/u^{*2} was required to reach a stationary state. The time interval used to calculate statistics was 715 ν/u^{*2}. Averaging was also carried out in the x and z directions so the results vary only with y. A memory of 2 gigabytes was required on a HP/Convex Exemplar-X. Computer runs were also carried out with grids of $128 \times 257 \times 128$ and $128 \times 193 \times 256$ to ensure adequacy of the resolution. These computations were performed for long enough time to get reasonable mean statistics up to second order. The results show the following: (a) A wall-normal resolution of 193 grids is required; higher resolution in this direction improves the mean temperature and root-mean square temperature fluctuation only slightly (peak rms temperature fluctuations differ by 1.6%). (b) The use of a higher resolution in the spanwise direction (256 grid points) does not produce significant changes to the first-order statistics. The turbulent Prandtl number near the wall decreased by about 2.7%.

The results for $Pr = 1$ and 3 were obtained for a $128 \times 129 \times 128$ grid for which Δy varied from 0.045 to 3.68. A time of about 1000 ν/u^{*2} was needed to reach a stationary state and averaging was done over periods of 750, 370 ν/u^{*2} for $Pr = 1.0$ and 3.0, respectively. A memory of 0.7 gigabytes was needed on a HP/Convex Exemplar-S.

3. Results from the DNS

3.1. Mean temperatures

Mean temperatures are presented in Fig. 1. The abscissa is the distance from the bottom wall made dimensionless with the friction velocity and the kin-

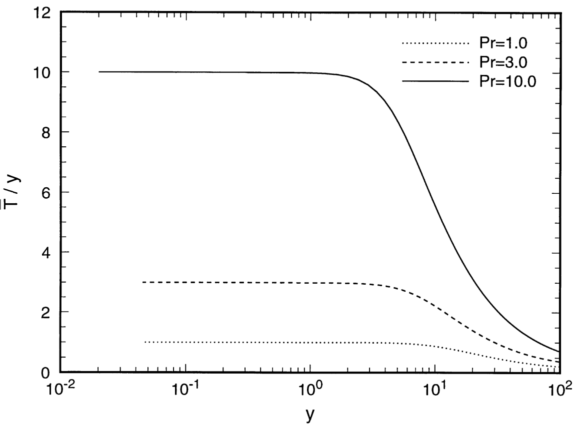

Fig. 1. Mean temperature profiles in semi-log coordinates, where $\bar{T}$ is made dimensionless with the friction velocity.

ematic viscosity. The ordinate is the mean temperature, made dimensionless with the friction temperature, divided by the dimensionless distance from the wall.

A conductive sublayer, where $\bar{T} = Pry$, exists close to the wall. The thickness of this sublayer, Δ_θ, decreases as Pr increases. That is, $\Delta_\theta = 6.0$, 3.6 and 1.9 for $Pr = 1$, 3 and 10. Over this range of Pr, thickness Δ_θ varies as $Pr^{-1/2}$.

3.2. Turbulent diffusivity

A turbulent diffusivity, defined as

$$\overline{\theta v} = -\frac{D^t}{\nu}\frac{d\bar{T}}{dy} \tag{5}$$

can be obtained from calculations of $\overline{\theta v}$ and $d\bar{T}/dy$. It can be also be calculated from a knowledge of $\bar{T}(y)$ and the heat flux, q_w. Since a fully-developed flow is considered,

$$q(y) = q_w = -\rho c_p (D + D^t)\frac{d\bar{T}}{dy}, \tag{6}$$

where all the terms are dimensional. This can be written in a non-dimensional form as

$$1 = -\left(\frac{1}{Pr} + \frac{D^t}{\nu}\right)\frac{d\bar{T}}{dy} \tag{7}$$

In the calculations, the same value of D^t was obtained from Eqs. (5) and (7) after a stationary state was reached.

Values of D^t for $Pr = 1$, 3, 10 are presented in Fig. 2. The dimensionless turbulent viscosity, ν^t/ν, was obtained from calculations made with a $128 \times 193 \times 128$ grid. The calculations seem to suggest that the turbulent diffusivity and the turbulent viscosity are equal for $y < 28$. However, a closer examination reveals that

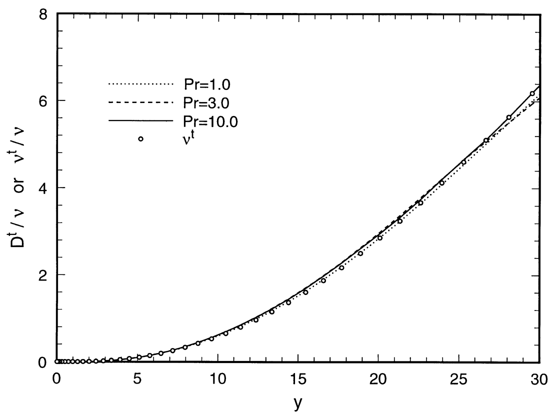

Fig. 2. Turbulent diffusivity and turbulent viscosity.

the turbulent Prandtl number, $Pr^t = \nu^t/D^t$, decreases with molecular Prandtl number, Pr, for $y < 10$.

3.3. Limiting behavior for $y \to 0$

The temperature profile for $Pr = 10$ in Fig. 1 shows that about 85% of the change occurs for $y < 20$, so the modeling of the region close to the wall is important. This becomes critical at larger Pr where the heat flux is quite small and the temperature gradients in the central regions (where D^t is large) are negligible. Therefore, it is of interest to give special consideration to the calculated temperature field close to the wall. If the fluctuating temperature and velocity fields are expanded in Taylor series, the following equations are obtained for a given Pr:

$$\theta = h_1 y + h_3 y^3 + \cdots \tag{8}$$

$$u = b_1 y + c_1 y^2 + d_1 y^3 + \cdots \tag{9}$$

$$v = c_2 y^2 + d_2 y^3 + \cdots \tag{10}$$

$$\overline{uv} = \overline{b_1 c_2} y^3 + \left(\overline{b_1 d_2 + c_1 c_2}\right) y^4 + \cdots \tag{11}$$

where the coefficients are functions of Pr and time t. There is no y^2 term in the equation for θ because $\partial^2\theta/\partial y^2$ is identically zero at the wall. Also,

$$\overline{\theta u} = \overline{h_1 b_1} y^2 + \overline{h_1 c_1} y^3 + \cdots \tag{12}$$

$$\overline{\theta v} = \overline{h_1 c_2} y^3 + \overline{h_1 d_2} y^4 + \cdots \tag{13}$$

$$\overline{\theta^2} = \overline{h_1^2} y^2 + \overline{h_1 h_3} y^4 + \cdots \tag{14}$$

The mean streamwise velocity is given as

$$\bar{U} = y - \frac{1}{2}\frac{y^2}{H} + \frac{1}{4}\overline{b_1 c_2} y^4 + \cdots \tag{15}$$

From Eqs. (5), (7) and (13), the following limiting expression is obtained for the mean temperature profile:

$$T_w - \bar{T} = Pry - \frac{Pr}{4}\overline{h_1 c_2} y^4 - \frac{Pr}{5}\overline{h_1 d_2} y^5 + \cdots \tag{16}$$

Values of $\sqrt{\overline{h_1^2}}$, $\sqrt{\overline{h_1^2}}/Pr$, $\overline{h_1 c_2}$, $\overline{h_1 c_2}/Pr$, $\overline{h_1 b_1}$, $\overline{h_1 b_1}/Pr$ are listed in Table 1. These parameters were calculated after the time averaged statistics were obtained. For instance, after dividing $\overline{\theta v}$ or Eq. (13), by y^3, one can easily get $\overline{h_1 c_2}$ by taking the limit of $y \to 0$ since only $\overline{h_1 c_2}$ survives on the right hand side of the resulting equation in the immediate vicinity of the wall.

Fig. 3 gives a plot of $\overline{\theta v}/y^3$ versus y. It is noted that

Table 1
Limiting values

Pr	1.0	3.0	10.0
$\sqrt{\overline{h_1^2}}$	0.403	1.22	3.93
$\sqrt{\overline{h_1^2}}/Pr$	0.403	0.405	0.393
$\overline{h_1 c_2} \times 10^{-3}$	0.730	2.09	5.03
$\overline{h_1 c_2}/Pr \times 10^{-4}$	7.30	6.98	5.03
$\overline{h_1 b_1}$	0.137	0.372	0.782
$\overline{h_1 b_1}/Pr$	0.137	0.124	0.0782

the region where $\overline{\theta v}$ varies with y^3 decreases with increasing Pr. More importantly, it is noted, from this figure, that this region lies within the conductive sublayer. Therefore, the first term in Eq. (13) is not having a direct role in determining the mean temperature profile. A plot of $(\overline{\theta^2})^{1/2}/y$ is given in Fig. 4. The regions in which $(\overline{\theta^2})^{1/2}/y$ is constant have slightly shorter extents than the regions where $(T_w - \bar{T})/y$ is constant (Fig. 1). A casual comparison of Figs. 1 and 4 suggests that $(\overline{\theta^2})^{1/2}/(T_w - \bar{T})$ for $y \to 0$ is independent of Pr and approximately equal to 0.40. However, the closer examination given in Table 1 indicates that $(\overline{\theta^2})^{1/2}/(T_w - \bar{T})$ could decrease slightly with increasing Pr for $Pr > 3$.

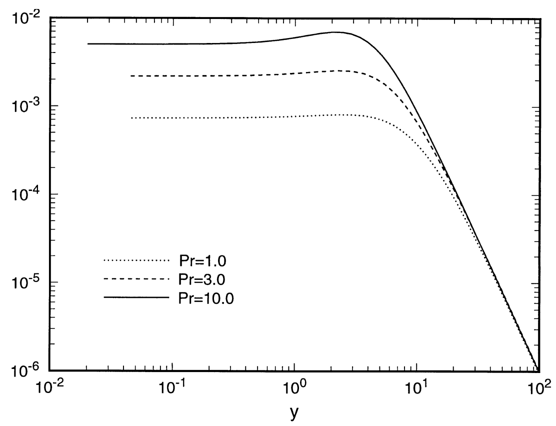

Fig. 3. Limiting behavior of $\overline{\theta v}$ near the wall.

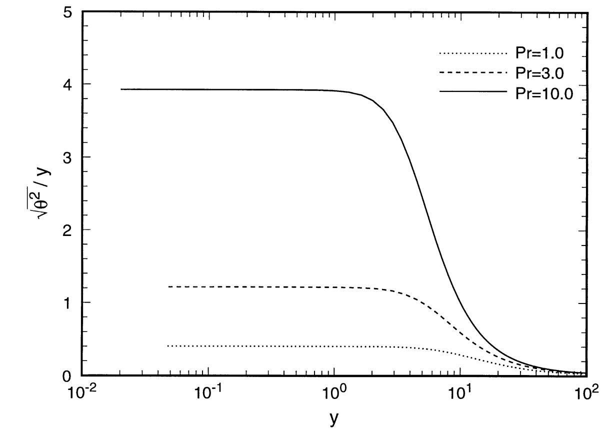

Fig. 4. Limiting behavior of $\sqrt{\overline{\theta^2}}$ near the wall.

The limiting behavior of D^t is given as

$$\frac{D^t}{\nu} = \frac{\overline{h_1 c_2}}{Pr} y^3 + \frac{\overline{h_1 d_2}}{Pr} y^4 - \frac{\overline{c_2 h_3}^2}{Pr} y^5 + \cdots \qquad (17)$$

From Table 1, it can be seen that the first term in Eq. (17) decreases with Pr. This is illustrated in Fig. 5 where D^t/ν is plotted against y for $Pr = 1$ and for $Pr = 10$. For $Pr = 1$ the limiting behavior of D^t is given as

$$\frac{D^t}{\nu} = 0.00073 y^3 \qquad (18)$$

This is approximately the same as the limiting behavior of ν^t

$$\frac{\nu^t}{\nu} = 0.00079 y^3 \qquad (19)$$

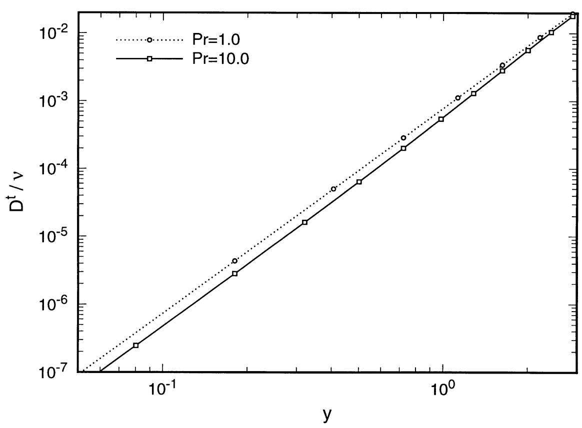

Fig. 5. Turbulent diffusivity close to the wall of the channel for $Pr = 1$ and 10.

The difference between Eqs. (18) and (19) might not be significant and could be the result of using different numbers of grid points. The limiting behavior for $Pr = 10$ is significantly different from the one for $Pr = 1$:

$$\frac{D^t}{\nu} = 0.00053y^3 \tag{20}$$

Since the region where $D^t/\nu \sim y^3$ decreases in size as Prandtl number increases, it might be expected from Eq. (17) that, in the limit of large Pr, it becomes vanishingly small (buried in a very thin conductive sublayer) and that $D^t/\nu \sim y^m$ over most of the scalar boundary layer, where m is greater than 3. For $Pr = 10$, Fig. 5 shows that D^t/ν varies roughly as $y^{3.4}$ over a large range of y. Thus, limiting relations (18) and (20) have very little effect on the mean temperature profile.

The following expression is obtained for the turbulent Prandtl number by using Eq. (17):

$$Pr^t = \frac{-\overline{b_1c_2}Pr - Pr\left[\overline{b_1c_2}/H + \left(\overline{b_1d_2 + c_1c_2}\right)\right]y + \cdots}{\overline{h_1c_2} + \overline{h_1d_2}y + \cdots} \tag{21}$$

The turbulent Prandtl number is given by $-\overline{b_1c_2}Pr/\overline{h_1c_2}$ in the limit of $y \to 0$. Since $\overline{b_1c_2}$ is constant for the Prandtl numbers considered, this leading term increases with Pr. This implies, for a given ν^t, that D^t decreases as Prandtl number increases. Thus, for $Pr \gg 1$, temperature (or concentration) fluctuations are greatly damped by molecular diffusion and the use of the analogy would lead to an inaccurate description of the behavior of D^t for $y \to 0$.

3.4. Spectra

The spectral density functions for $\overline{\theta^2}$ are compared to those for the normal velocity fluctuations at $y = 0.2$ in Fig. 6. It is noted, at large wavenumbers, that fluctuations in the temperature at $Pr = 1$ are strongly damped relative to fluctuations in the normal velocity. An increase in Pr is associated with a further damping. This is better seen in Figs. 7 and 8 where the cumulative contributions of different wavenumbers to $\overline{\theta^2}$ and $\overline{\theta v}$, at $y = 0.2$, are shown.

Spectra at larger y are different from those in the immediate vicinity of the wall. This is illustrated in Figs. 9 and 10, which give plots of the cumulative spectral density at $y = 25$. These clearly show that the contribution from high wavenumbers to $\overline{\theta^2}$ increases in importance as Pr increases. However, the influence of Pr on the cumulative spectral density function for $\overline{\theta v}$ is relatively small. This is because high wavenumbers do not contribute significantly to $\overline{v^2}$ as they do to $\overline{\theta^2}$ at large Pr. Thus, one can expect the correlation, $\overline{\theta v}/(\overline{\theta^2})^{1/2}(\overline{v^2})^{1/2}$, to decrease as Pr increases at locations that are not close to the wall.

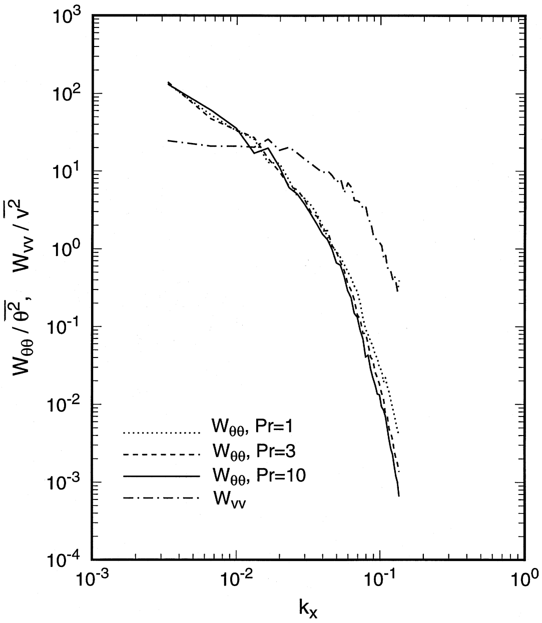

Fig. 6. Spectral density functions for $\overline{\theta^2}$ at $y = 0.2$.

4. Mass transfer at large Schmidt number

Eulerian methods cannot be used to calculate temperature fields at large Pr with presently available computers. However, Papavassiliou and Hanratty [12,13] have shown how Lagrangian calculations can be carried out if a DNS of the velocity field is available. Some of their results for a channel flow, at $H = 150$, are given in Fig. 11 as points. It is noted that all of the

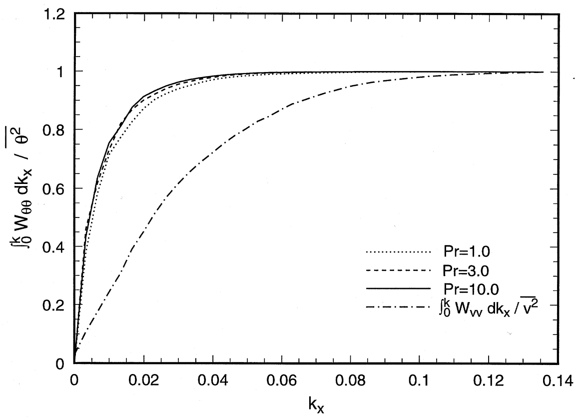

Fig. 7. Cumulative spectral density functions of $\overline{\theta^2}$ at $y = 0.2$.

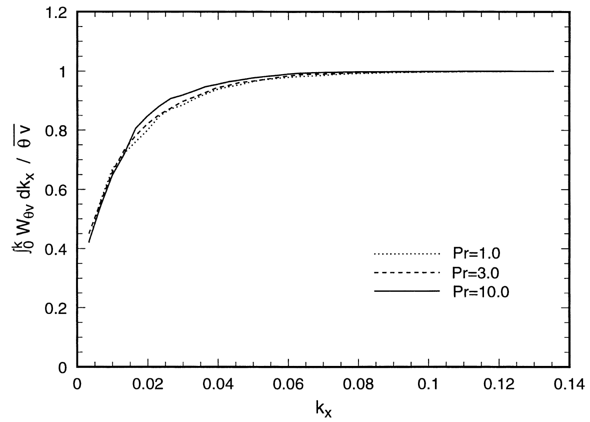

Fig. 8. Cumulative spectral density functions for $\overline{\theta v}$ at $y = 0.2$.

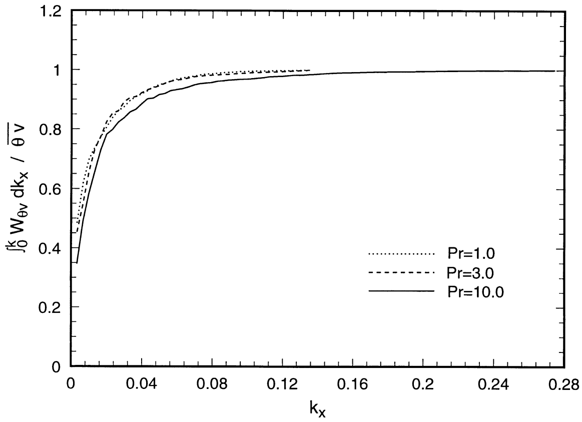

Fig. 10. Cumulative spectral density functions for $\overline{\theta v}$ at $y = 25$.

temperature change occurs within the viscous sublayer at $Pr = 100$, 500, 2400.

The dashed lines were calculated by assuming the $D^t = \nu^t$ [15] over the values of y where the concentration is changing. The analogy clearly does not predict the influence of Pr shown in Fig. 11. The solid curves were calculated by assuming $D^t/\nu = 0.000463y^{3.38}$. This produces the following relation for the mass transfer coefficient made dimensionless with the friction velocity:

$$\frac{\bar{K}}{u^*} = 0.0889Sc^{-0.704} \tag{22}$$

This is in excellent agreement with the extensive laboratory measurements presented by Shaw and Hanratty [9] and the recent results of Papavassiliou and Hanratty [13].

Values of D^t, calculated with the temperature profiles in Fig. 11 and Eq. (7), are compared with the DNS results (for $Pr = 1$ and 10) in Fig. 12. Because D^t was not obtained from direct measurements of Reynolds transport, Papavassiliou and Hanratty [13] were not able to obtain values in the conductive sublayer. That is, the limiting behavior of D^t for $y \rightarrow 0$ cannot be obtained from the calculations of the profiles of average concentration. However, this figure shows that the equation $D^t/\nu = 0.000463y^{3.38}$ represents an interpolation between the limiting behavior at very small y and the region where $D^t = \nu^t$.

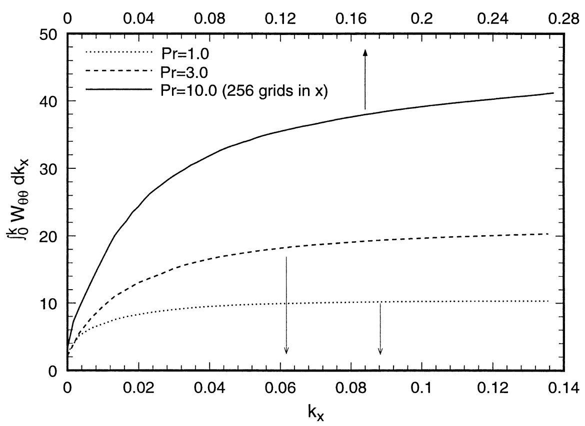

Fig. 9. Cumulative spectral density functions of $\overline{\theta^2}$ at $y = 25$.

Frequency spectra for high Sc obtained by Shaw and Hanratty [16] are compared with the present DNS result for $Pr = 10$ in Fig. 13. An increase in Schmidt number is associated with a marked decrease in the frequency of the mass transfer fluctuations. The mean frequency, defined as

$$\langle n \rangle = \frac{1}{\overline{\theta^2}} \int_0^\infty n W_{\theta\theta} \, dn, \tag{23}$$

decreases as the Schmidt or Prandtl number increases and has a value of about 9.4×10^{-3} for $Pr = 10$. The concentration boundary layer acts as a filter so the concentration field does not respond to high frequency velocity fluctuations. This damping increases with Schmidt number. For high Sc, the spectral function for the velocity fluctuations close to a wall is found to be constant over the range of frequencies characterizing the mass transfer fluctuations. However, this is not the case for $Pr = 10$ (see Fig. 13).

Sirkar and Hanratty [17] have argued that the spectral density function for mass transfer fluctuations, W_{kk}, at large frequencies is represented by a solution of a simplified linear form of the mass balance equation for concentration c,

$$\frac{\partial c}{\partial t}\left[1 - \frac{\bar{U}}{U_c}\right] - D\frac{\partial^2 c}{\partial y^2} = -v\frac{d\bar{C}}{dy}, \tag{24}$$

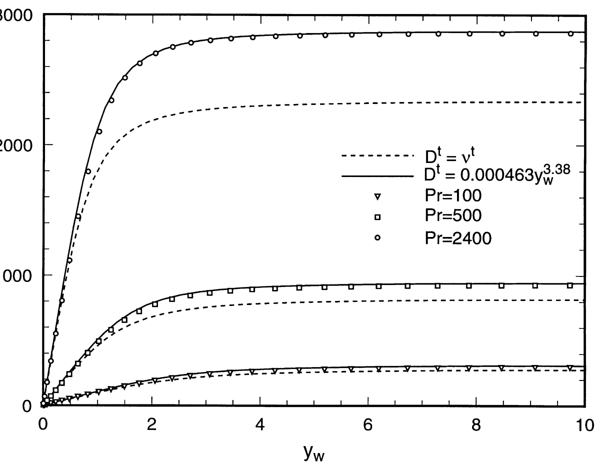

Fig. 11. Dimensionless mean temperature profiles for high Pr.

where the following substitution is made:

$$\frac{\partial}{\partial x} = -\frac{1}{U_c}\frac{\partial}{\partial t} \tag{25}$$

In order to solve Eq. (24), Sirkar and Hanratty approximated $d\bar{C}/dy$ with $\bar{K}/Sc$ and assumed $[1 - \bar{U}/U_c] \approx 1$. From this simplified form of Eq. (24), Shaw and Hanratty [16] obtained the following relation between the spectral density functions for the velocity, W_{vv}, and concentration fluctuations.

$$W_{kk} = \frac{4W_{vv}/y^4\bar{K}^2}{Sc(2\pi n)^3} \tag{26}$$

This shows the strong damping of concentration fluctuations close to the wall since $W_{kk} \sim W_{vv}/n^3$. Furthermore, the appearance of Sc in the denominator reveals that the filtering increases with increasing Schmidt number. For very large Sc, for which W_{vv} is a constant, Eq. (26) predicts $W_{kk}/\bar{K}^2$ varies as $(n^3 Sc)^{-1}$, in agreement with measurements. Calculated values of the dimensionless spectral density function of the temperature fluctuations at $y = 0.02$ for $Pr = 10$ that have been normalized with $\bar{T}^2$ are also plotted in Fig. 14. These also show a -3 slope at large n, but they fall below the experimental data when plotted in the manner suggested by Eq. (26).

Shaw and Hanratty [16] obtained $W_{vv}(0)/y^4 = 9.8 \times 10^{-3}$ from the data in Fig. 14 for high frequencies and Eq. (26). This value is larger than the one obtained from the DNS data (2.3×10^{-3}) shown in

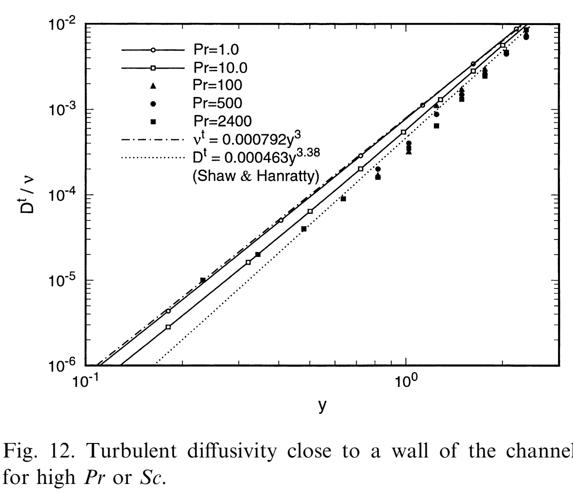

Fig. 12. Turbulent diffusivity close to a wall of the channel for high Pr or Sc.

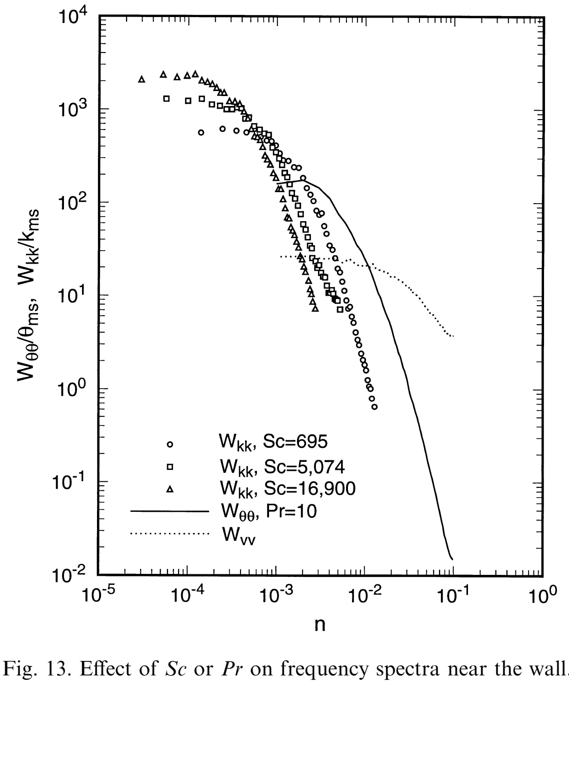

Fig. 13. Effect of Sc or Pr on frequency spectra near the wall.

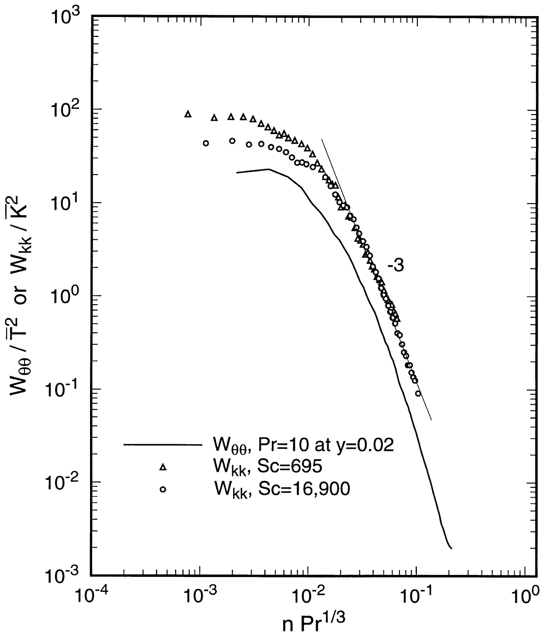

Fig. 14. Frequency spectra plotted in accordance with Eq. (26).

Fig. 13. A plausible explanation is that errors are introduced by the assumption of $[1 - \bar{U}/U_c] \approx 1$. If $[1 - \bar{U}/U_c]$ is represented by an effective average of 0.62, the spectral density function for $Pr = 10$ agrees with Eq. (24) at high frequencies. Vassiliadou's study [18] of convection velocities of the concentration field for high Sc gives $U_c \approx 5$ for $Sc = 1000$. Thus, $\bar{U}/U_c \approx 0.38$ gives $\bar{U} \approx 1.9$, which corresponds to a velocity inside the very thin conductive layer. Figs. 15 and 16 give $\phi(k_x, n)$ and U_c calculated at $y = 0.02$ for $Pr = 10$. The convection velocities in Fig. 15 were calculated by the following definition given by Wills [19]:

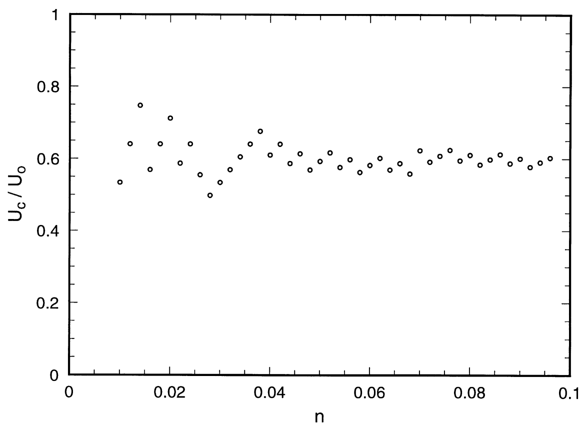

Fig. 15. Convection velocities in the near-wall temperature field at $Pr = 10$, made dimensionless by centerline velocity, $U_0 = 17.8$.

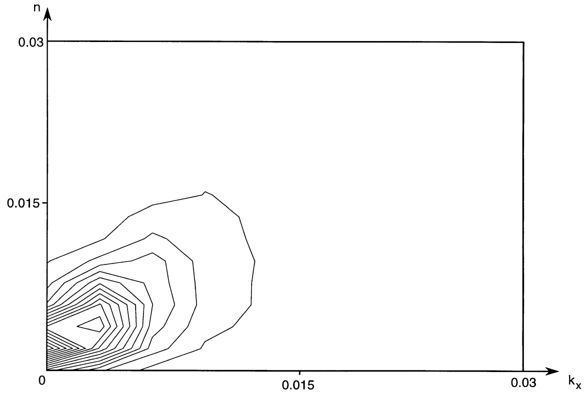

Fig. 16. Contours of the wavenumber–frequency spectral density function, $\phi(k_x, n)$, of the temperature fluctuations for $Pr = 10$ and $y = 0.02$. Contour levels are from 0.5 to 16.5. Increments of 0.5 are used.

$$U_c(k_x) = \frac{n_c(k_x)}{k_x} \tag{27}$$

where

$$\left[\frac{\partial \phi(k_x, n)}{\partial n}\right]_{n=n_c(k_x)} = 0 \tag{28}$$

Here, $\phi(k_x,n)$ is the two-dimensional spectral density function of the temperature field in the immediate vicinity of the wall. A value of $\bar{U}/U_c \approx 0.38$ corresponds to $\bar{U} \approx 3.9$ since $U_c \approx 10.3$. This seems reasonable since $\bar{U} \approx 3.9$ corresponds to the edge of the conductive layer in which the mean temperature shows a linear behavior.

5. Discussion

For $Pr \geq 1$ and for $y > 5$, the influence of Prandtl number on D^t is quite small. A corollary of this observation is that the use of a turbulent Prandtl number to relate scalar transport to the velocity field could be a sensible approach. In fact, the assumption that $D^t = \nu^t$ is a good approximation in the viscous wall region beyond $y = 5$ and in the log-layer. In the outer flow, $D^t > \nu^t$ and the turbulent Prandtl number depends on the boundary conditions.

At small y the turbulent diffusivity increases as y^3 for all Pr. However, $D^t/\nu y^3$ decreases weakly with increasing Pr as $y \rightarrow 0$. This can be understood if it is recognized that temperature fluctuations in this region are mainly governed by fluctuations in the rate of heat transfer at the wall, rather than hydrodynamic mixing of hot and cold fluids.

The thickness of the region where $D^t/\nu \sim y^3$ decreases with increasing *Pr*. However, it always lies in the conductive sublayer where turbulent transport is negligible compared to molecular transport; that is, turbulence in this region is not directly influencing the mean temperature profile. For very large *Pr* almost all of the temperature change occurs in the viscous sublayer where $\nu^t/\nu \sim y^3$. Because of this, the argument is commonly made that temperature or concentration profiles can be calculated by assuming $D^t/\nu \sim y^3$. The results outlined above suggest that this approach is incorrect.

Close to the wall, fluctuations in temperature are more damped at high wavenumbers than are fluctuations in the normal velocity. Thus, the contribution from high wavenumbers to $\overline{\theta v}$ is relatively small. This explains why the analogy between momentum and heat or mass transfer cannot be used to define the limiting behavior of D^t for $y \rightarrow 0$. The behavior at larger y is strikingly different from what is found in the immediate vicinity of the wall since the contribution from high wavenumbers to $\overline{\theta^2}$ increases in importance as *Pr* increases.

The major contribution of this paper is that it challenges theoretical notions that are a bulwark of present analyses of turbulent scalar fields. The limiting behavior of D^t for $y \rightarrow 0$ cannot be given by using the $\nu^t/\nu \sim y^3$ relation and the analogy between momentum and scalar transport. This limiting relation for D^t cannot be used to describe turbulent transport at large *Sc* or *Pr* since it is applicable only in the conductive sublayer where turbulent transport is not important.

Acknowledgements

This work has been supported by the National Science Foundation through grant CTS-95-03000. Computer resources have been provided by the National Center for Supercomputer Applications (NCSA), Urbana and the Computing Center at University of Kentucky, Lexington.

References

[1] A.S. Monin, A.M. Yaglom, in: Statistical Fluid Mechanics: Mechanics of Turbulence, 1, MIT Press, Cambridge, MA, 1971, pp. 343–347.
[2] D.B. Spalding, Unified theory of friction, heat transfer and mass transfer in the turbulent boundary layer and wall jet, Aero. Res. Counc., Rep. No. 25 (1975) 925.
[3] R.A. Antonia, J. Kim, Turbulent Prandtl number in the near-wall region of a turbulent channel flow, Int. J. Heat Mass Transfer 34 (7) (1991) 1905–1908.
[4] S.W. Churchill, New simplified models and formulations for turbulent flow and convection, A.I.Ch.E.J. 33 (5) (1997) 1125–1140.
[5] V.G. Levich, Physicochemical Hydrodynamics, Prentice-Hall, Englewood Cliffs, NJ, 1962.
[6] P. Harriott, R.M. Hamilton, Solid–liquid mass transfer in turbulent pipe flow, Chem. Engng. Sci 20 (12) (1965) 1073–1078.
[7] B.A. Kader, Temperature and concentration profiles in fully turbulent boundary layers, Int. J. Heat Mass Transfer 24 (9) (1981) 1541–1544.
[8] J.S. Son, T.J. Hanratty, Limiting relation for the eddy diffusivity close to a wall, A.I.Ch.E.J. 13 (4) (1967) 689–696.
[9] D.A. Shaw, T.J. Hanratty, Turbulent mass transfer to a wall for large Schmidt numbers, A.I.Ch.E.J. 23 (1) (1977) 28–37.
[10] J.A. Campbell, T.J. Hanratty, Mechanism of turbulent mass transfer at a solid boundary, A.I.Ch.E.J. 29 (1983) 221.
[11] T.J. Hanratty, E. Vassiliadou, Turbulent transfer to a wall at large Schmidt numbers, in: Hirata, N. Kasagi (Eds.), Transport Phenomena in Turbulent Shear Flows. Theory, Experiment and Numerical Simulation, Hemisphere, New York, 1988, pp. 255–274.
[12] D. Papavassiliou, T.J. Hanratty, The use of Lagrangian methods to describe turbulent transport of heat from a wall, Industrial Engineering Chemical Research 34 (1995) 3359–3367.
[13] D. Papavassiliou, T.J. Hanratty, Transport of a passive scalar in a turbulent channel flow, Int. J. Heat Mass Transfer 40 (6) (1997) 1303–1311.
[14] S.L. Lyons, T.J. Hanratty, J.B. McLaughlin, Large-scale compter simulation of fully developed turbulent channel flow with heat transfer, Numerical Methods with Fluids 13 (1991) 999–1028.
[15] O. Reynolds, On the extent and action of the heating surface for steam boilers, Proc. Manchester Lit. Phil. Soc. 14 (1874) 7–12.
[16] D.A. Shaw, T.J. Hanratty, Influence of Schmidt number on the fluctuating of turbulent mass transfer to a wall, A.I.Ch.E.J. 23 (2) (1977) 160–169.
[17] K.K. Sirkar, T.J. Hanratty, Relation of turbulent mass transfer to a wall at high Schmidt numbers to the velocity field, J. Fluid Mech 44 (1970) 589–603.
[18] E. Vassiliadou, Turbulent mass transfer to a wall at large Schmidt numbers, Ph.D. thesis, University of Illinois, Urbana, IL, 1985.
[19] J.A.B. Wills, Measurements of the wave-number/phase velocity spectrum of wall pressure beneath a turbulent boundary layer, J. Fluid Mech 45 (1970) 65–90.